

In conclusion, we have demonstrated a hybrid-memory device where information can be introduced optically and can be extracted or erased electrically. We expect much improved performance, in terms of retention, stability, and operating voltages upon introducing intentional electron-trapping centers in dilute proportions in the semiconducting-polymer matrix, along with optimization of geometrical parameters.

Experimental

The top-contact geometry, as shown in Figure 1a, was used to fabricate the polymer field-effect transistor devices based on poly(3-hexylthiophene) (P3HT) [7]. Regioregular P3HT was obtained from Aldrich Inc., and was re-purified using standard procedures (re-precipitation method). Our samples and devices were handled in a glove box (MBraun, Inc.), and stringent procedures were observed to ensure the quality of the devices. A transparent water-soluble dielectric (polyvinyl alcohol, $\epsilon \approx 8$) layer with a thickness of 0.5 μm was spin-coated on top of an aluminum-coated glass substrate. The dielectric surface was then treated using standard established procedures using hexamethyldisilazane. A layer of regioregular P3HT (thickness ≈ 150 nm) was spin-coated (1500 rpm) from chloroform solution on the insulator under an inert atmosphere, followed by a thermal treatment under vacuum at 60 $^{\circ}\text{C}$ for 24 h. The drain and source electrodes with a separation of 25–40 μm (L) and width of 2 mm (W) were deposited by thermal evaporation of gold using a shadow mask. All the experiments were performed under vacuum (10^{-1} Pa).

Received: January 20, 2004
Final version: July 23, 2004

- [1] K. S. Narayan, N. Kumar, *Appl. Phys. Lett.* **2001**, *79*, 1891.
- [2] L. Torsi, A. Dodabalapur, H. E. Katz, *J. Appl. Phys.* **1995**, *78*, 1088.
- [3] Z. Bao, A. Dodabalapur, A. J. Lovinger, *Appl. Phys. Lett.* **1996**, *69*, 4108.
- [4] A. R. Brown, C. P. Jarrett, D. M. de Leeuw, M. Matters, *Synth. Met.* **1997**, *88*, 37.
- [5] G. Horowitz, *Adv. Mater.* **1998**, *10*, 365.
- [6] H. J. Queisser, D. E. Theodorou, *Phys. Rev. B: Condens. Matter Mater. Phys.* **1986**, *33*, 4027.
- [7] S. Dutta, K. S. Narayan, *Phys. Rev. B: Condens. Matter Mater. Phys.* **2003**, *68*, 125 208.
- [8] E. J. Meijer, C. Detcheverry, P. J. Baesjou, E. van Veenendaal, D. M. de Leeuw, T. M. Klapwijk, *J. Appl. Phys.* **2003**, *93*, 4831.
- [9] S. Dutta, Th. B. Singh, K. S. Narayan, *Synth. Met.* **2003**, *139*, 553.

Ultrahigh-Density Arrays of Ferromagnetic Nanorings on Macroscopic Areas**

By Frank Q. Zhu,* Donglei Fan, Xiaochun Zhu, Jian-Gang Zhu, Robert C. Cammarata, and Chia-Ling Chien

Nanoscale magnetic entities play a prominent role in many devices in which the shape and dimension of the entities dictate their intricate magnetization configurations and switching characteristics.^[1–4] Of particular interest are small circular disks that can acquire the so-called vortex state, in which the magnetic flux is confined within the magnetic entity and creates no stray fields,^[5–10] so that the cross-talk between entities can be reduced. However, the vortex core (with magnetization pointing out of the plane of the disk) tends to destabilize the vortex state, which consequently is replaced by the single-domain state in sufficiently small disks. In supermalloy disks, the transition from vortex state to single-domain state occurs at a diameter of a few hundred nanometers.^[11,12] However, the instability of the vortex core in a small circular disk can be circumvented by removing the central region of the disk to form a ring structure.^[13–15] Small magnetic nanorings can not only maintain stable vortex states, but also hold the potential for information storage in the two chiralities of the circulating magnetization. These properties of nanorings have also led to the proposal of high-density, vertical, magnetic, random access memory (VMRAM)^[16] consisting of multilayered nanorings with exceptional stability and desirable switching characteristics.

For these reasons, the study of magnetic nanorings of various sizes has been actively pursued recently. Electron-beam lithography (EBL) is one method used for fabricating magnetic nanorings.^[17–24] The magnetic nanorings should have good uniformity in ring size and ring cross-section, lest the domain walls be pinned at the locations of the deviations. Most of the magnetic rings previously reported have been in the mi-

[*] Dr. F. Q. Zhu, Prof. C.-L. Chien
Department of Physics and Astronomy
Johns Hopkins University
3400 N. Charles St.
Baltimore, MD 21218 (USA)
E-mail: qzhu@pha.jhu.edu

Dr. D. Fan, Prof. R. C. Cammarata
Department of Materials Science and Engineering
Johns Hopkins University
3400 N. Charles St.
Baltimore, MD 21218 (USA)

Dr. X. Zhu, Prof. J.-G. Zhu
Department of Electrical and Computer Engineering
Carnegie Mellon University
5000 Forbes Ave.
Pittsburgh, PA 15213 (USA)

[**] This research is financially supported by NSF and DARPA.

rometer-size range, with few reports existing on sub-micrometer-sized nanorings. The arrays of magnetic rings made by EBL usually have a small number of rings (e.g., less than 10^3) with low areal densities (e.g., $0.5 \text{ rings } \mu\text{m}^{-2}$ or less^[19]). As such, the magnetic signal of the magnetic nanorings has been too weak for full characterization using magnetometry. Instead, the magnetic characteristics have been measured or inferred by surface magneto-optic Kerr effect (MOKE) measurements,^[17,19] resistance measurements,^[18,22] Hall-sensor measurements,^[20,24] and magnetic force microscopy.^[21] In these cases, the external applied magnetic field could only be applied in certain directions, and not all, so as not to interfere with the specific measuring technique used.

Alternatively, nanorings can be made using templates, such as nanosphere templates^[25] and porous templates.^[26] There has also been a report of triangular nanoplates being made by chemical synthesis.^[27] In this work, we use a nanosphere-template method, where one relies on the assembly of a large number of monodisperse nanospheres to produce a large number of uniform, magnetic nanorings. We have fabricated a large number ($\sim 10^9$) of Co nanoring magnets with inner diameters of 100 nm over a macroscopic area ($\sim 1 \text{ cm}^2$) with a very high areal density ($45 \text{ rings } \mu\text{m}^{-2}$), while maintaining good spatial and dimensional uniformity. Because of the large number of uniform rings, the switching characteristics can be readily measured in detail by a vibrating sample magnetometer (VSM) and compared with micromagnetics simulations.

Our process uses monodisperse polystyrene (PS) nanospheres as templates, as schematically shown in Figure 1. A monolayer of PS nanospheres (100 nm in diameter) was first formed on the substrate (Fig. 1a) by manipulating its surface chemistry. A thin film, in our case a Co film, was then sputter-deposited onto the substrate (Fig. 1b). The thickness of the Co layer can be any value up to the radius of the PS nanospheres. Ar^+ ion-beam etching, with a normally incident beam and a pre-calibrated etching rate, was then used to remove all the deposited Co, except that under the nanospheres. This resulted in an array of Co nanorings as shown in Figure 1c. The PS nanospheres may be left on the rings or be chemically removed. A thin protective layer (e.g., Au) can also be deposited over the entire surface (Fig. 1d). The size of the nanorings and the areal density of the arrays were dictated by those of the PS-nanosphere template, whereas the compositions and thickness of the nanorings were controlled by the deposition process. The nanorings may be made of a single material or a multilayer consisting of different materials, with a total thickness less than the radius of the PS spheres. The nanorings thus fabricated, and especially the thick ones, had a tapered cross-section (Fig. 1e).

Scanning electron micrographs of the arrays of Co nanorings (Figs. 2a–c) show a large number of nanorings uniformly distributed over the substrate without piling or contacts between the rings. The outer diameters (140 nm), the inner diameters (100 nm), and the ring widths (20 nm) of these Co nanorings had very narrow distributions. The presence of the nanospheres at the center of the nanorings is revealed in

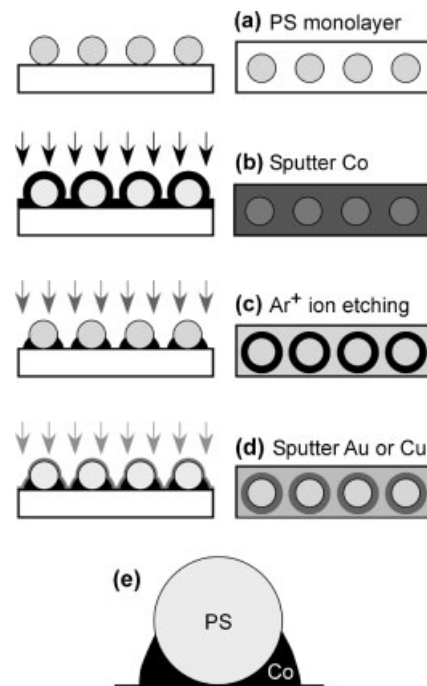


Figure 1. Schematic of the fabricating process for arrays of nanorings shown from a side view (left column) and a top view (right column): a) a monolayer of polystyrene (PS) nanospheres is deposited onto the substrate; b) a thin film of Co is sputter-deposited over the surface and PS nanospheres; c) an Ar^+ ion beam is used, in normal incidence, to etch away the sputtered Co film and thus leaving only the nanorings protected under the PS nanospheres; d) a capping layer of Au or Cu is deposited over the entire surface to prevent oxidation. e) Schematic of the tapered cross-section of a nanoring.

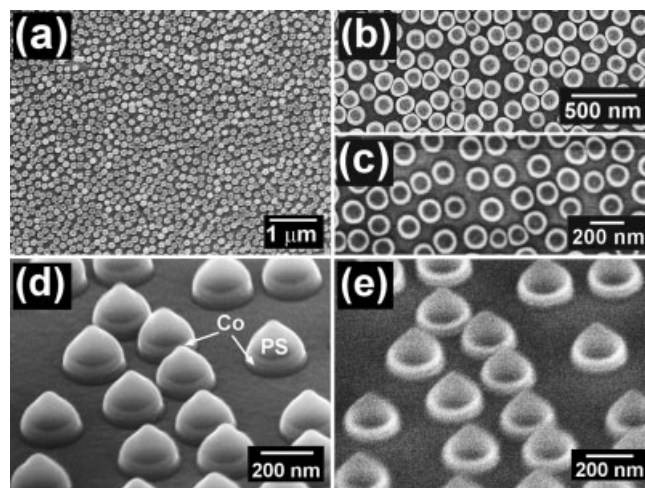


Figure 2. a–c) Top-view scanning electron micrographs of the Co nanorings made from 100 nm diameter PS spheres. d,e) 50° tilted view of nanorings made from 200 nm diameter PS spheres. The images in (c) and (e) are collected by a back-scattered-electron detector, whose contrast was determined by the atomic-weight difference between PS and Co.

Figures 2d,e which were obtained by tilting the substrate by 50° . An areal density of $45 \text{ rings } \mu\text{m}^{-2}$, or $4.5 \times 10^9 \text{ rings cm}^{-2}$,

was determined from Figure 2a. The diameters and widths of these nanorings are among the smallest reported, and the arrays also have the largest number of nanorings and largest areal density reported.

The PS spheres can be chemically decomposed by heating to 300 °C in an oxygen atmosphere for 30 min. The bare Co rings as seen in Figure 3a have a tapered profile, as further illustrated in an enlarged micrograph (Fig. 3b), where the inner parts are darker (i.e., they are lower in height) than the outer parts

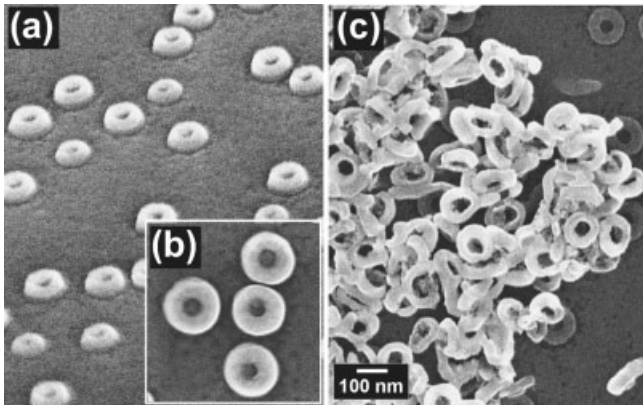


Figure 3. a) Tilted-view micrograph of the Co rings after annealing in oxygen. b) Close-up of the bare Co rings. c) A collection of Co rings freed from the substrate.

parts. When the Co rings were freed from the substrate by external forces, the rings aggregated, as shown in Figure 3c, and the shapes of the rings could be viewed from all directions.

The large number of Co nanorings in a specimen of area 3 mm × 3 mm was readily accessible using conventional magnetometric techniques. We used a vector vibrating sample magnetometer (VSM) (ADE model 10) so that the components of magnetization parallel (*x*-component) and perpendicular (*y*-component) to the magnetic field were measured simultaneously at room temperature with the magnetic field in the plane of the substrate. Before etching out the Co nanorings, measurements were made on the continuous Co film covering the PS nanospheres, which showed a hysteresis loop typical of a ferromagnetic thin film with a coercivity of 9.5 mT. In contrast, the Co nanorings showed a completely different hysteresis loop as shown in Figure 3a. From the measured saturation magnetization of 0.24×10^{-3} emu ($1 \text{ emu} = 10^{-3} \text{ A m}^2$), the dimensions of the nanorings, and the specimen size, we have determined an areal density of 49 rings μm^{-2} , which is in good agreement with the value of 45 rings μm^{-2} determined in one small region from scanning electron microscopy. This indicates that the arrays of nanorings had a uniform, high, areal density over a macroscopic area of about 1 cm^2 .

The hysteresis loop of the Co nanorings shown in Figure 3a has several unique characteristics. It shows a squareness (defined as the ratio of remnant magnetization, M_r , to saturation

magnetization, M_S) of about 0.65. There are two switching fields, one at about 16.3 mT and the other at a much higher value of 0.2 T. Between the two switching fields, there is a plateau of relatively unvarying magnetization. The *y*-component is always nearly zero at all field values. When the magnetic field was applied in other directions in the sample plane, both loops of the *x*- and the *y*-components were essentially the same as those shown in Figure 3a. The absence of in-plane anisotropy is a manifestation of the uniformities in ring size and ring width among the rings in the array.

In order to understand the details of the switching processes, we resorted to micromagnetic simulations of Conanoring arrays that had the same dimensions, thicknesses, and tapered cross-sections as the actual Co nanorings in this study. A micromagnetic model based on the Landau–Lifshitz–Gilbert equation^[28] was used with a saturation magnetization, $M_S = 1440 \text{ emu cm}^{-3}$, and a ferromagnetic exchange-energy constant $A_{\text{ex}} = 1.6 \times 10^{-6} \text{ erg cm}^{-1}$ ($1 \text{ erg} = 10^{-7} \text{ J}$). Within each mesh cell of the simulated model, the magnetostatic field was averaged volumetrically. Curved edges in the nanorings were approximated by staircased, square, mesh cells, which was effectively an artificially built-in edge roughness. The detailed computational methods have been described in a previous publication.^[29]

The simulation showed that there are two parallel switching processes. The first switching process leads to the vortex state as shown in Figure 4a. From the right onion state (OR) at a

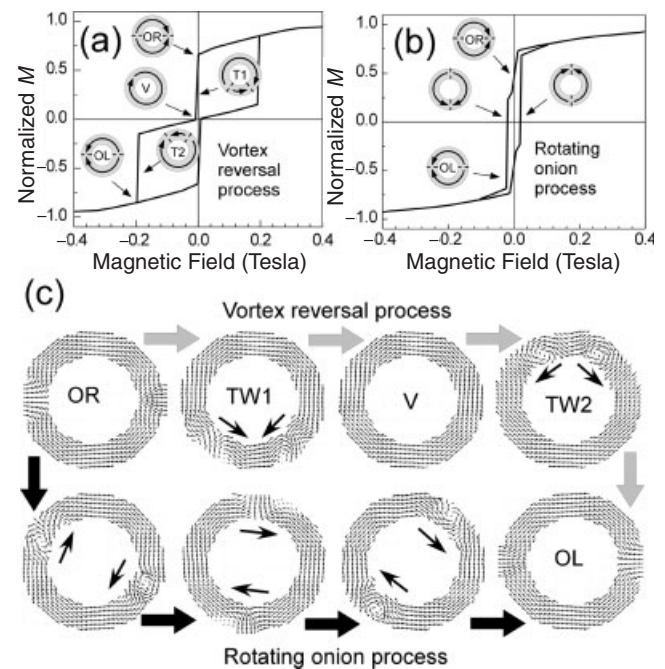


Figure 4. Micromagnetics simulations reveal that there are two parallel magnetic reversal processes: a) a vortex-reversal process with two switching fields of 5 mT and 0.2 T, between which the magnetization of the vortex state is essentially zero; and b) a rotating-onion process with a switching field of 15 mT. Both processes have a squareness of 64%. c) Different evolutions of the magnetic states through vortex-reversal and rotating-onion processes.

small negative field, the two domain walls move towards each other, forming a twisted state 1 (TW1) (also reported previously^[30]). The two domain walls quickly annihilate to reach the vortex state (V) at 5 mT. The vortex state, with nearly zero magnetization, is very stable and can withstand large magnetic fields. Only at a large field of 0.2 T are two new domain walls initiated to form the twisted state 2 (TW2), and then pushed towards the two sides to become the left onion state (OL). The transition from the onion state to the vortex state is the better-known switching process for nanorings.

The micromagnetic simulations have also revealed another switching process, the rotating onion process, as shown in Figure 4b. After the onion state is reached, the two domain walls maintain their 180° separation and do not annihilate each other. Instead, under a small magnetic field, they move in unison within the nanoring. The configuration changes from the right onion state (OR) to the left onion state (OL) by rotations of 180° of both walls. This rotation can be either clockwise or counterclockwise. This process has a coercivity of about 15 mT and does not lead to the vortex state.

Reversal via either the vortex formation process or the rotation of the onion state is determined by the relative motion of the two domain walls at the onset of reversal. An attractive motion of the two domain walls, or two opposite magnetic poles, at the onset of reversal leads to the vortex reversal process. The micromagnetic simulations show that, in a ring with large thickness or width, the large magnetostatic energy between the two domain walls favors the vortex process. In a ring of small thickness or width, the Zeeman energy becomes dominant during reversal, in which case the two domain walls are more likely to move with the same helicity, yielding the rotating onion state. For rings of intermediate thickness or width, as is the case here, the Zeeman energy and the magnetostatic energy are comparable. The local pinning of the domain walls becomes important in determining the initial relative motion of the two domain walls at the onset of reversal, leading to one or the other switching process. The simulations show that the probabilities for the two processes occurring are roughly the same. The relative probability can be more accurately determined from experimental measurements.

The actual hysteresis loop of about 10⁹ Co nanorings, as shown in Figure 5a, is a weighted composite of two separate loops of the two switching processes shown in Figures 4a,b. The experimental results can be very well reproduced by the theoretical loop shown in Figure 5b which is a composite of 40 % of the vortex reversal process (Fig. 4a) and 60 % of the rotating onion process (Fig. 4b), with switching fields, H_C , at 14.2 mT and 0.2 T. It may be noted that the remnant state of both switching processes is the onion state. One can easily calculate that it has an effective magnetization of $(2/\pi)M_0 \approx 64\%$, which is in excellent agreement with the experimental result of 65 % squareness. The simulations also revealed that both switching processes have zero y -components, as observed. It should be emphasized that the micromagnetic simulations have not only revealed the details of the two parallel switching processes, but have also quantitatively repro-

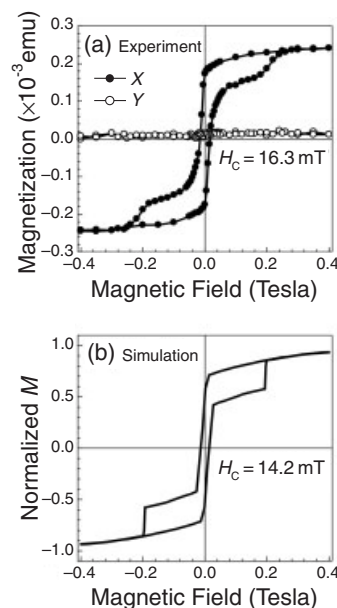


Figure 5. a) Room-temperature magnetic hysteresis loops of Co nanorings with inner diameters of 100 nm and widths of 20 nm, simultaneously measured parallel (x -component, solid circles) and perpendicular (y -component open circles) to the magnetic field. b) Hysteresis loop determined by the micromagnetic simulation, using 40 % vortex-reversal process and 60 % rotating-onion process.

duced the experimentally observed loop shape, as well as the actual switching fields. Finally, despite the high density of the nanorings, the simulations showed that interactions among the nanorings are insignificant, even for the rotating onion process.

In summary, we have fabricated and studied, using magnetometry, arrays of 10⁹ Co nanorings with inner diameters of 100 nm, widths of 20 nm, and with a high areal density of 45 rings μm^{-2} . We have observed two parallel switching processes: the vortex reversal process and the rotating onion process. Micromagnetic simulations of the quantitative details were in excellent agreement with the experimental results.

Experimental

PS Coating: PS spheres of concentrations 2.5 wt.-% in water purchased from Alfa Aesar were diluted to 0.125 wt.-% with de-ionized (DI) water and then applied to a (001) Si substrate (after proper surface processing). The sample was then rinsed with DI water and blow-dried with dry N₂ gas.

Sputter Coating: A Co film was sputter-deposited from a 99.995 % pure Co target in a magnetron sputtering system with 6×10^{-8} torr (1 torr \approx 133.3 Pa) base pressure and 6 mtorr Ar-sputtering pressure. The motions of the samples and shutter were all computer-controlled. Film thicknesses were measured using a small-angle X-ray reflectivity technique on a Philips X'Pert 4-circle diffraction system.

Ion-Beam Etching: A Veeco 3 cm direct-current Ar⁺ ion source was used to perform the etching of the Co. The working conditions were 500 V beam current, 66 mA beam current, 1000 V acceleration voltage, and 0.23 mtorr Ar-pressure. The calibrated etching rate of the Co was 10.54 Å s⁻¹.

Scanning Electron Microscopy: JEOL 6700F scanning electron microscope with 2.2 nm resolution and a Robinson backscatter-electron detector was used to study the morphology of the samples.

Vector Vibrating Sample Magnetometry: We used an ADE model 10 VSM with a rotating magnet to measure the *x*- and *y*-components simultaneously. The instrument had a 10^{-6} T field resolution, $\pm 1.5\%$ magnetization accuracy, and $\pm 1.5^\circ$ angle accuracy.

Received: May 4, 2004

Final version: September 3, 2004

Oriented Sexiphenyl Single Crystal Nanoneedles on TiO₂ (110)**

By Georg Koller,* Stephen Berkebile, Joachim R. Krenn, George Tzvetkov, Gregor Hlawacek, Ondrej Lengyel, Falko P. Netzer, Christian Teichert, Roland Resel, and Michael G. Ramsey

- [1] M. Hehn, K. Ounadjela, J. P. Bucher, F. Rousseaux, D. Decanini, B. Bartenlian, C. Chappert, *Science* **1996**, 272, 1782.
- [2] K. J. Kirk, J. N. Chapman, S. McVitie, P. R. Aitchison, C. D. W. Wilkinson, *Appl. Phys. Lett.* **1999**, 75, 3683.
- [3] M. Herrmann, S. McVitie, J. N. Chapman, *J. Appl. Phys.* **2000**, 87, 2994.
- [4] C. A. Ross, *Annu. Rev. Mater. Res.* **2001**, 31, 203.
- [5] M. Demand, M. Hehn, K. Ounadjela, R. L. Stamps, E. Cambriil, A. Cornette, F. Rousseaux, *J. Appl. Phys.* **2000**, 87, 5111.
- [6] T. Shinjo, T. Okuno, R. Hassdorf, K. Shigeto, T. Ono, *Science* **2000**, 289, 930.
- [7] M. Schneider, H. Hoffmann, J. Zweck, *Appl. Phys. Lett.* **2001**, 79, 3113.
- [8] A. Wachowiak, J. Wiebe, M. Bode, O. Pietzsch, M. Morgenstern, R. Wiesendanger, *Science* **2002**, 298, 577.
- [9] L. D. Buda, I. L. Prejbeanu, U. Ebels, K. Ounadjela, *J. Magn. Magn. Mater.* **2002**, 242, 996.
- [10] M. Rahm, M. Schneider, J. Biberger, R. Pulwey, J. Zweck, D. Weiss, V. Umansky, *Appl. Phys. Lett.* **2003**, 82, 4110.
- [11] R. P. Cowburn, D. K. Koltsov, A. O. Adeyeye, M. E. Welland, D. M. Tricker, *Phys. Rev. Lett.* **1999**, 83, 1042.
- [12] R. P. Cowburn, D. K. Koltsov, A. O. Adeyeye, M. E. Welland, D. M. Tricker, *Phys. Rev. Lett.* **1999**, 81, 5414.
- [13] M. Kläui, C. A. F. Vaz, L. Lopez-Diaz, J. A. C. Bland, *J. Phys.: Condens. Matter* **2003**, 15, R985.
- [14] S. P. Li, D. Peyrade, M. Natali, A. Lebib, Y. Chen, U. Ebels, L. D. Buda, K. Ounadjela, *Phys. Rev. Lett.* **2001**, 86, 1102.
- [15] J. Rothman, M. Kläui, L. Lopez-Diaz, C. A. F. Vaz, A. Bleloch, J. A. C. Bland, Z. Cui, R. Speaks, *Phys. Rev. Lett.* **2001**, 86, 1098.
- [16] J. G. Zhu, Y. Zheng, G. A. Prinz, *J. Appl. Phys.* **2000**, 87, 6668.
- [17] L. J. Heyderman, C. David, M. Kläui, C. A. F. Vaz, J. A. C. Bland, *J. Appl. Phys.* **2003**, 93, 10011.
- [18] M. Kläui, C. A. F. Vaz, J. A. C. Bland, W. Wernsdorfer, G. Faini, E. Cambriil, L. J. Heyderman, *Appl. Phys. Lett.* **2003**, 83, 105.
- [19] Y. G. Yoo, M. Kläui, C. A. F. Vaz, L. J. Heyderman, J. A. C. Bland, *Appl. Phys. Lett.* **2003**, 82, 2470.
- [20] J. Bekaert, D. Buntinx, C. Van Haesendonck, V. V. Moshchalkov, J. De Boeck, G. Borghs, V. Metlushko, *Appl. Phys. Lett.* **2002**, 81, 3413.
- [21] M.-F. Lai, C.-R. Chang, J. C. Wu, Z.-H. Wei, J. H. Kuo, J.-Y. Lai, *IEEE Trans. Magn.* **2002**, 38, 2550.
- [22] S. Kasai, E. Saitoh, H. Miyajima, *J. Appl. Phys.* **2003**, 93, 8427.
- [23] U. Welp, V. K. Vlasko-Vlasov, G. W. Crabtree, J. Hiller, N. Zaluzec, V. Metlushko, B. Ilic, *J. Appl. Phys.* **2003**, 93, 7056.
- [24] M. Steiner, J. Nitta, *Appl. Phys. Lett.* **2004**, 84, 939.
- [25] J. Aizpurua, P. Hanarp, D. S. Sutherland, M. Käll, G. W. Bryant, F. J. García de Abajo, *Phys. Rev. Lett.* **2003**, 90, 57401.
- [26] K. L. Hobbs, P. R. Larson, G. D. Lian, J. C. Keay, M. B. Johnson, *Nano Lett.* **2004**, 4, 167.
- [27] Y. Sun, Y. Xia, *Adv. Mater.* **2003**, 15, 695.
- [28] J.-G. Zhu, Y. Zheng, in *Spin Dynamics in Confined Magnetic Structures I*, (Eds: B. Hillebrands, K. Ounadjela), Springer-Verlag, Heidelberg, Germany **2002**, p 289.
- [29] J.-G. Zhu, Y. Zheng, X. Lin, *J. Appl. Phys.* **1997**, 81, 4336.
- [30] F. J. Castaño, C. A. Ross, C. Frandsen, A. Eilez, D. Gil, H. I. Smith, M. Redjfal, F. B. Humphrey, *Phys. Rev. B* **2003**, 67, 184425.

Thin films of conjugated organic materials as the active layer in electronic and optoelectronic devices have attracted considerable interest for more than a decade. The growth of highly oriented crystalline films is of particular interest as this may lead to improved performance in organic thin film transistors (OTFTs) or organic light-emitting diodes (OLEDs).^[1,2] Moreover, the ability to grow oriented crystalline structures on a nanometer scale will be a prerequisite for the advent of organic nanotechnology. In the present paper we have investigated *para*-sexiphenyl (*p*-6P: C₃₆H₂₆) films grown via physical vapor deposition onto a TiO₂ (110) single crystal substrate. *Para*-sexiphenyl is of technological relevance since it is used as the active material in blue-light-emitting diodes, and is also considered to be a promising material for solar cells.^[3,4] The TiO₂ substrate is interesting because it is an optically clear insulating oxide, which can be n-doped via heat treatment in ultra-high vacuum (UHV) to become conductive. Moreover, the TiO₂(110) orientation is highly anisotropic and can thus be used as a template for crystalline film growth. Here, we show that at room temperature *p*-6P forms highly oriented nanoneedles from the initial stages of growth to thin films. Although the growth of *p*-6P needles has been reported on the dielectrics mica and alkali halides,^[5-9] these needles consist of numerous crystallite orientations.^[9] In contrast, the *p*-6P nanoneedles on TiO₂ presented here display only a single crystalline orientation, the *p*-6P(20 $\bar{3}$). These *p*-6P(20 $\bar{3}$) crystallites are exclusively oriented along the TiO₂[1 $\bar{1}$ 0] substrate azimuth. All the molecules are perfectly parallel to each other, to the substrate surface and to the TiO₂[001] azimuthal direction, with their molecular planes all having the same angle of $\pm 34^\circ$ with respect to the substrate surface plane.

[*] Dr. G. Koller, S. Berkebile, Dr. J. R. Krenn, Dr. G. Tzvetkov, Prof. F. P. Netzer, Prof. M. G. Ramsey
Institute of Physics, Karl-Franzens-University
A-8010 Graz (Austria)
E-mail: georg.koller@uni-graz.at

G. Hlawacek, Prof. C. Teichert
Institute of Physics, University of Leoben
A-8700 Leoben (Austria)
Mr. O. Lengyel, Prof. R. Resel
Institute of Solid State Physics, Graz University of Technology
A-8010 Graz (Austria)

[**] This work was supported by the Austrian Science Foundation (FWF). The able assistance of Denis Vyalikh at RG-BL of BESSY is also gratefully acknowledged.